Desert Research Institute

TECHNICAL MEMORANDUM

To: Jean Moran, Stetson Engineers

From: Chris Garner, Steve Bacon, Greg Pohll, and Jenny Chapman

Date: November 17, 2017

Re: Indian Wells Valley Groundwater Model Update

This technical memorandum details updates to the Indian Wells Valley Groundwater Model since the last model report was released in 2016 (McGraw, 2016).

The primary motivation for this model update is to correct the under prediction in El Paso Valley (EPV) by incorporating regional faults as groundwater barriers. This work is supported by a detailed structural analysis of the basin that was performed by DRI to map fault structures that act as groundwater barriers. In addition, pre-development (1920s) and more recent groundwater levels were processed to remove duplicate and erroneous data. This model update includes a full calibration of both steady-state (pre-development) and transient (1920 – 2016) models. A predictive simulation was developed to provide future estimates of drawdown 100 years into the future. The predictive simulation assumed current pumping conditions that continue into the future.

Attached are two digital files that represent the transient historical water budget:

- DRI_IWVtr.out – MODFLOW list file in asci format.
- DRI_IWV-TransientWaterBudget.xlsx – Transient water budget in Excel format.

Desert Research Institute
www.dri.edu
2215 Raggio Parkway
Reno, NV 89512

Introduction

The Indian Wells Valley (IWV) groundwater basin in California has been in overdraft since the 1960s (Dutcher and Moyle, 1973). The limitations of sustainable groundwater resources in the valley were recognized as early as 1912 (Lee, 1912). The primary consumption of groundwater is for municipal and agricultural uses. Under current rates, pumping exceeds basin yield by a factor of three to five and the result is a decline in groundwater levels on the order of 1 – 2 feet per year. The Desert Research Institute (DRI) developed and calibrated a steady-state and transient groundwater flow model to predict water level changes in the future (McGraw et. al, 2016). The area being simulated by the groundwater model is shown in Figure 1.

Though the previous version of the DRI model (McGraw et al., 2016) showed improved predictability throughout most of model domain as compared to an earlier version (Brown and Caldwell, 2009), predicted water levels in El Paso Valley were under predicted by hundreds of feet. The poor calibration in El Paso Valley was due to a lack of pre-development water level measurements in this area and the absence of regional faults that are now known to act as groundwater barriers.

The primary motivation for this model update is to correct the under prediction in El Paso Valley by incorporating regional faults as groundwater barriers. This work is supported by a detailed structural analysis of the basin that was performed by DRI to map fault structures that act as groundwater barriers. In addition, pre-development (1920s) and more recent groundwater levels were processed to remove duplicate and erroneous data. This model update includes a full calibration of both steady-state (pre-development) and transient (1920 – 2016) models. A predictive simulation was developed to provide future estimates of drawdown 100 years into the future. The predictive simulation assumed current pumping conditions that continue into the future.

Structural Geology

An analysis of active faulting within IWV was performed to define faults that are acting as groundwater barriers. The IWV model domain is located within a tectonically active area of California referred to as the northern portion of the Eastern California shear zone or southern Walker Lane (e.g., Dokka and Travis, 1990; Wesnousky, 2005). The valley floor of Indian Wells Valley is cross-cut by a northerly trending mosaic of fault segments with a wide-range of fault activity that merge towards the north with the Sierra Nevada frontal fault system and Coso Range (e.g., Hauksson et al., 1995). Active faults in IWV that are known to act as groundwater barriers, thereby increasing horizontal hydraulic gradients, include the Little Lake fault zone (LLFZ) and a fault that crosses the eastern margin of El Paso Valley within the southwestern sector of the model domain (Figure 2). The later fault is informally referred to as the El Paso fault (EPF) in this study

The LLFZ and EPF are mapped having an activity of <15,000 years (USGS, 2006) (Figure 2 and Figure 3). In the vicinity of the mapped EPF, a large groundwater head gradient is present with head declines on the order of 100 ft/mile (Brown and Caldwell, 2009). The high gradient has been attributed to faulting, concentration of low permeability sediments, reduced vertical cross sectional flow area, and deep fracture flow from the wetter western slope of the Sierra Nevada (Thyne *et al.*, 1999). The location and strike of the inferred section of fault is based on the position of the local groundwater level from

nearby wells, but there is some uncertainty as to its exact location which is why it is shaded in Figures 2 and 3.

Observations and modeling of the groundwater system in Owens Valley, which is the next major hydrographic basin north of IWV, have shown that fault systems can reduce transmissivity of aquifer materials in fault zones by a factor of 20 – from 80,000 to 4,000 (gal/d)/ft (Danskin, 1998). Findings from the structural analysis indicate that the LLFZ and the EPF represent barriers to groundwater flow. Inclusion of these faults improves the conceptual model of the valley and increase the accuracy of simulated water levels in El Paso Valley. The LLF and the EPF are modeled in the horizontal flow barrier (HFB) package as five different fault segments (Figure 4) and are assumed to penetrate to alluvial sediments and bedrock.

Water Level Targets

Pre-Development

The available pre-development water level dataset was revised to include 132 steady-state water level calibration targets (Figure 5). The wells were selected to provide adequate spatial coverage of pre-development aquifer levels while also eliminating redundancy and measurements that deviated substantially from the regional head gradients indicated by adjacent wells. Because pre-development water levels at specific monitoring wells were not recorded in El Paso Valley, recent but stable water levels in this region were used to represent pre-development conditions. Water level targets in El Paso Valley that were used in the previous version of the model (McGraw et al., 2016) were based on interpolated values developed by Brown and Caldwell, 2009. Therefore, four wells were identified that demonstrated stable water levels. The mean value of head over the period of record for each well was set as the pre-development water level target in calibration (Table 1).

Table 1. Wells and water levels used to represent pre-development conditions in El Paso Valley.

Well #	Water Level (ft)
28S38E18R	2818.2
27S38E27M01	2677.1
27S38E21L01	2660.8
27S38E08R01	2696.9

Post-Development

Similar to the pre-development water level target dataset, the post-development data were re-examined to eliminate redundancy and erroneous measurements. The locations of the resulting water level targets are shown in Figure 6.

Groundwater Production Data

The Indian Wells Valley Cooperative Groundwater Management Group (IWVCGMG) maintains a record of annual production (http://iwvgroundwater.org/iwv-production-data/) for the agricultural,

private domestic, municipal, Naval Air Weapons Station China Lake (NAWS), and Searles Valley Minerals (SVM) use from 1975 to 2015. Post-1975 annual model groundwater production for each of these categories is compared to the total IWVCGMG annual production shown in Figure 7. On average, total model pumping is less than the IWVCGMG totals by 1,300 acre-feet per year. Todd, 2014 noted that the higher rates associated with the IWVCGMG estimate is a result of potential overlap with agriculture and overestimation of the water demand. The single well rate used in the DRI model is approximately 1 acre-feet per year rather than 2.5 acre-feet per year prescribed in the IWVCGMG estimate. The lower rate used herein is more consistent with the Todd, 2014 analysis which suggests the rate is generally less than 1 acre-feet per year, with only a few parcels that exceed this amount. The agricultural, municipal, NAWS, and SVM production showed good correspondence to the IWVCGMG records.

Groundwater pumping for each well was extended through 2016 based on annual production data provided by local water purveyors and estimates for agricultural production. Agricultural wells associated with developing Pistachio orchards were updated to reflect an increasing water demand as the orchards mature as was done in the previous version of the DRI model (McGraw et al., 2016). For NAWS and the IWVWD, production data were available for individual wells. Only total annual production was available for SVM, the City of Inyokern, Ridgecrest Heights, City of Ridgecrest, and private domestic wells, so production was distributed equally to all wells in each category. The location of each production well is provided in Figure 8.

Model Calibration

Steady-State

The PEST (Parameter Estimation) software (Doherty and Hunt, 2010) was used to calibrate the steady-state model. Calibration was achieved by adjusting the spatial distribution of horizontal hydraulic conductivity in the upper three layers using the pilot point methodology. The pilot-point methodology (Doherty, 2003) is applied to develop a heterogeneous hydraulic conductivity field that yields an acceptable agreement between the simulated and measured hydraulic heads.

The hydraulic conductivity in the lower 3 layers of the model was adjusted by PEST using a zonation approach. Two homogeneous hydraulic conductivity zones were developed. One zone represents all of IWV and the other for EPV with the dividing line being the EPF.

The hydraulic characteristic parameter was also adjusted during the calibration for the horizontal flow barriers representing faults. The LLFZ was subdivided into three segments and the EPF into two segments as shown in Figure 4. Each segment was assigned a unique hydraulic characteristic value to achieve agreement between simulated and measured groundwater levels.

Transient

The specific yield (Sy) and specific storage (Ss) were adjusted during the calibration to match measured drawdown rates and absolute water levels at the monitoring well locations shown in Figure 6. No additional adjustment to the hydraulic conductivity field calibrated in the steady-state model was required for the transient calibration.

The transient calibration covered the period 1921 through 2016. The calibration metrics (drawdown rate and water level) were found to be insensitive to specific storage so this value was held constant at $3x10^{-7}$ ft^{-1}.

Because transient water level data often contain outliers due to measurement errors, a robust regression approach was implemented that dynamically removes outliers from the drawdown slope calculation so that a more representative slope of drawdown could be estimated.

Ordinary least squares regression assumes a normal distribution of errors in the observed responses. If the data to be fitted contain erroneous or stress affected measurements, the resulting slope fit will be skewed by the outlier data points. A robust regression fit is better suited to these circumstances because the approach automatically removes outlier observations within the analysis period by assigning a weight to each data point. The weights are iteratively recomputed to exclude data points farther from model predictions.

For each simulated variation in the specific yield parameter, the difference in the slope of the head observations and the simulated head values is computed using Equation 1:

$$MAE_{slope} = \frac{1}{n}\sum_{w=0}^{n} abs\{[\log(abs(S_{sim})) - \log(abs(S_{obs}))]\} \quad (1)$$

where MAE_{slope} = mean absolute error in the drawdown slope, n = number of monitoring wells, S_{sim} = drawdown slope (simulated), and S_{obs} = drawdown slope (observed). It was necessary to take the logarithm of the data to reduce the inherent bias of comparing values that span several orders of magnitude. This *MAE* results from taking the difference in logs and has no units.

The mean absolute error (*MAE*) in the absolute water level was also calculated using the following equation:

$$MAE_{water\ level} = \frac{1}{n}\sum_{w=0}^{n} abs\{h_{sim} - h_{obs}\} \quad (2)$$

where $MAE_{water\ level}$ = mean absolute error in the water level, n = number of water level measurements wells, h_{sim} = simulated groundwater level, and h_{obs} = measured groundwater level.

Results

Steady-State

The automated calibration process yielded a hydraulic conductivity field and fault characteristics used in the horizontal flow barrier package. The calibrated hydraulic conductivity field for layers 1 to 3 is provided in Figure 9. The hydraulic conductivity values range from 0.003 ft/day to 20 ft/day. Calibrated hydraulic conductivity values for layers 4 to 6 were 0.03 ft/day and 1 ft/day in EPV and IWV, respectively. PEST optimized fault characteristics are shown in Table 2.

A one to one plot of the observed versus simulated heads is provided in Figure 10. *MAE* error for the steady state model is 6 ft and relative error which is the *MAE* divided by the range in observed head is 0.84 percent. Typically, models that have a relative error less than 10 percent are deemed acceptable

for predictive purposes. Models with a relative error less than 5 percent are considered excellent (Anderson *et al*., 2015).

Figure 11 shows the residual in the simulated versus observed groundwater level for the steady-state model. Green dots indicate simulated head greater than the observed and red dots indicate simulated head less than the observed. The size of the dots is proportional to the absolute residual. Note that there is significant improvement in the magnitude of the water level residual in El Paso Valley as compared to the previous version of the model. In some cases, the transient model differed from measurements by as much as 300 – 400 ft. The updated version of the model shows better agreement with residuals ranging between 5 – 30 ft. It is also important to note that the hydraulic gradients are very steep in the vicinity of the EPF which can lead to larger errors because of small errors the in spatial position of monitoring wells and the inability to resolve sub-grid gradients.

Table 2. Calibrated fault characteristics.

Fault Segment	Fault Characteristic (day^{-1})
Little Lake North	6.8×10^{-4}
Little Lake Central	1.3×10^{-3}
Little Lake South	4.1×10^{-4}
El Paso North	1.2×10^{-5}
El Paso South	1.9×10^{-5}

The steady-state water budget is provided Table 3. The sole inflow to the steady-state model is mountain block recharge which equals 7,645 afy. Evapotranspiration (7,546 afy) is the primary outflow with a small component of interbasin outflow (100 afy) between IWV and Searles Valley.

Table 3. Simulated steady-state water budget.

INPUTS	
	Amount (acre-ft/year)
Natural recharge	7,645
Total:	7,645
OUTPUTS	
	Amount (acre-ft/year)
ET	7,546
Interbasin flow	100
Total:	7,646

Transient

An example result from the robust regression slope fitting approach for California state well number (SWN) 26S39E26B02 is shown in Figure 12. Red dots represent the observed water levels, blue

the simulated water levels, yellow and green represent the observed and simulated water levels that were inputs to the regression model, and hollow black dots and solid black dots correspond to outliers identified in the observed and simulated, respectively. Note that two observations prior to 1994 were excluded from the regression analysis of this well. For this example, outliers were identified by the robust regression approach in the observations and in the simulated heads. The observed drawdown slope is -2.28 ft/yr and the simulated slope is -2.89 ft/year corresponding to a slope difference of -0.70 ft/year. Simulated and measured groundwater level hydrographs over the transient calibration period (1921 – 2016) are provided for all monitoring wells used in the transient calibration in Appendix A.

The *MAE* in drawdown slope for each of the specific yield parameter values tested is shown in Figure 13. Using *MAE* of drawdown slope as the calibration metric, the best fitting specific yield is 0.2. Figure 14 shows the *MAE* in absolute groundwater levels for various specific yield values. The optimal solution (minimum error) is achieved with a specific yield of 0.2. Therefore, both calibration metrics yield an optimal specific yield value of 0.2. Note that removal of outliers does not impact the optimal specific yield and only has a minimal impact on the error metric. A map of the drawdown slope difference (simulated – observed in units of feet per year) at each well for Sy = 0.2 is shown in Figure 15.

Predictive

A predictive scenario was simulated to assess potential for drawdown if the system were to continue status quo groundwater production for 100 years ending in 2116. Contour maps of total drawdown at 10, 25, 50, and 100 years into the future are provided in Figures 16, 17, 18, and 19 respectively. A contour map of the drawdown rate after 100 years is provided in Figure 20. Maximum simulated drawdown after 100 years exceeds 160 feet on the west-central boundary of the model domain in the vicinity of Brown road. Other more localized drawdown cones are located near higher rate production wells. Changes in drawdown across the LLF are in the range of 50 feet and drawdown does not propagate significantly into EPV.

References

Brown and Caldwell, 2009. Final Report, Indian Wells Valley Basin Groundwater Flow Model and Hydrogeologic Study, Prepared for the Indian Wells Valley Water District, Ridgecrest, CA.

Bryant, W.A., and Hart, E.W., 2007. Fault rupture hazard zones in California: Alquist-Priolo earthquake fault zoning act with index to earthquake fault zones maps. California Geological Survey Special Publication 42, 42 p.

Danskin, W.R., 1998. Evaluation of the hydrologic system and selected water-management alternatives in the Owens Valley, California, USGS Water Supply Paper 2370-H

Doherty, J., 2003. Ground water model calibration using pilot points and regularization, Ground Water, 41(2), pp. 170-177.

Doherty, J.E., and R.J. Hunt, 2010. Approaches to highly parameterized inversion—A guide to using PEST for groundwater-model calibration: U.S. Geological Survey Scientific Investigations Report 2010–5169, 59 p

Dokka, R.K., and Travis, C.J., 1990. The role of the Eastern California shear zone in accommodating Pacific–North American plate motion. Geophysical Research Letters 17, 1323–1326.

Dutcher, L.C., and W.R. Moyle, Jr. 1973. “Geologic and Hydrologic Features of the Indian Wells Valley, California.” USGS Water Supply Paper 2007.

Hauksson, E., Hutton, K., Kanamori, H., Jones, L., Mori, J., Hough, S., and Roquemore, G., 1995. Preliminary report on the 1995 Ridgecrest earthquake sequence in eastern California. Seismological Research Letters 66, 54–60.

Lee, C.H., 1912. Ground-water resources of Indian Wells Valley, California, California State Conservation Commission Report, p. 403-429.

McGraw, D., R. Carroll, G. Pohll, J. Chapman, S. Bacon, and R. Jasoni, 2016. Groundwater Resource Sustainability: Modeling Evaluation for the Naval Air Weapons Station, China Lake, California, Prepared by Desert Research Institute for the Naval Air Warfare Center Weapons Division, China Lake, CA, NAWCWD TP 8811.

Thyne, G.D., J.M. Gillespe, and J.R. Ostdick, 1999. Evidence for interbasin flow through bedrock in the southeastern Sierra Nevada, Geological Society of America Bull. 111 (11): 1600-1616.

Todd, 2014. Indian Wells Valley Resource Opportunity Plan Water Availability and Conservation Report, Report submitted to Kern County Planning and Community Development Department.

USGS [U.S. Geological Survey and California Geological Survey], 2006. Quaternary fault and fold database for the United States, accessed April 14, 2009, from USGS web site: http//earthquake.usgs.gov/hazards/qfaults/.

Wesnousky, S.G., 2005. Active faulting in the Walker Lane. Tectonics, 24, TC3009, doi: 10.1029/2004TC001645.

Figures

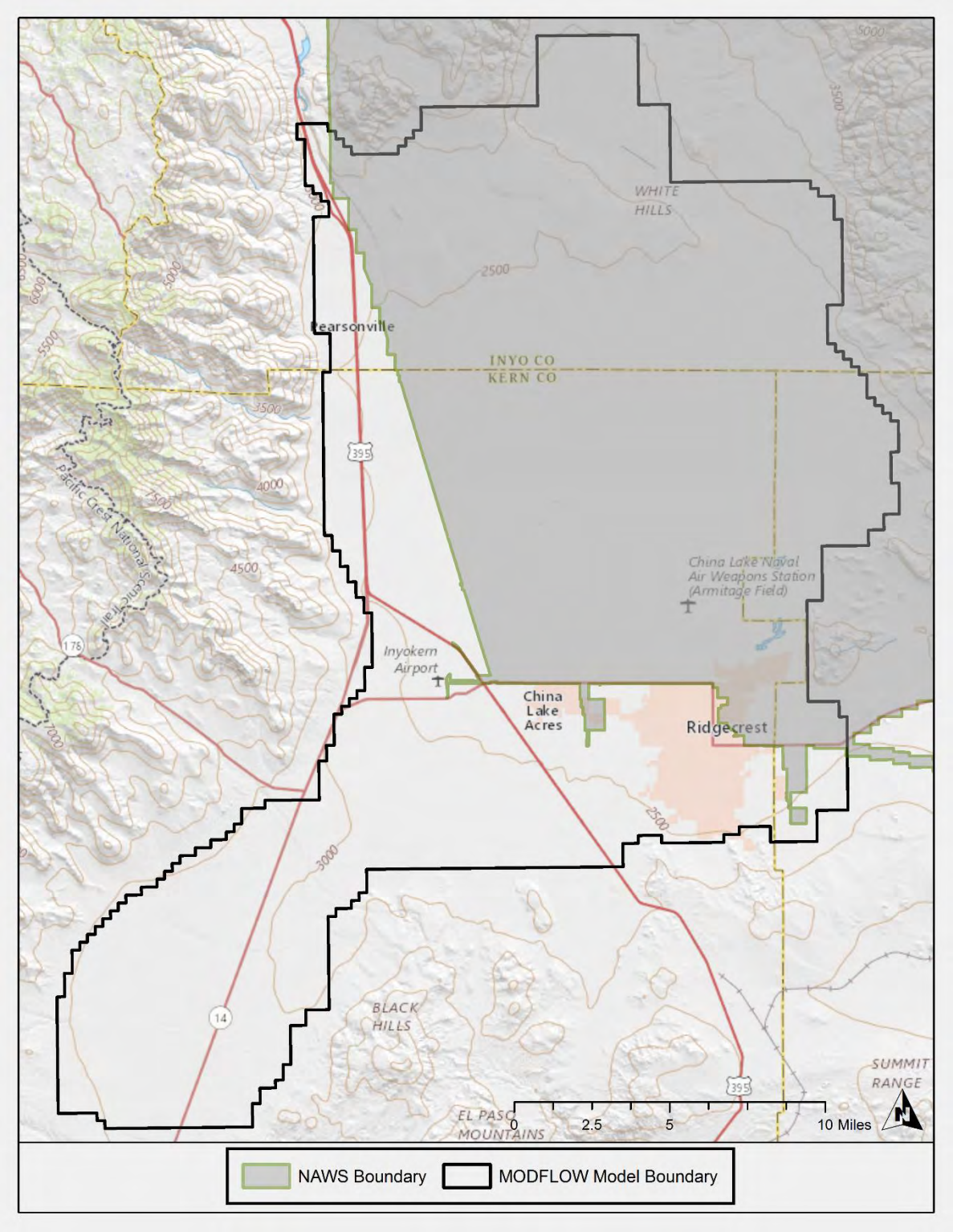

Figure 1. Indian Wells Valley groundwater flow model boundary and NAWS boundary.

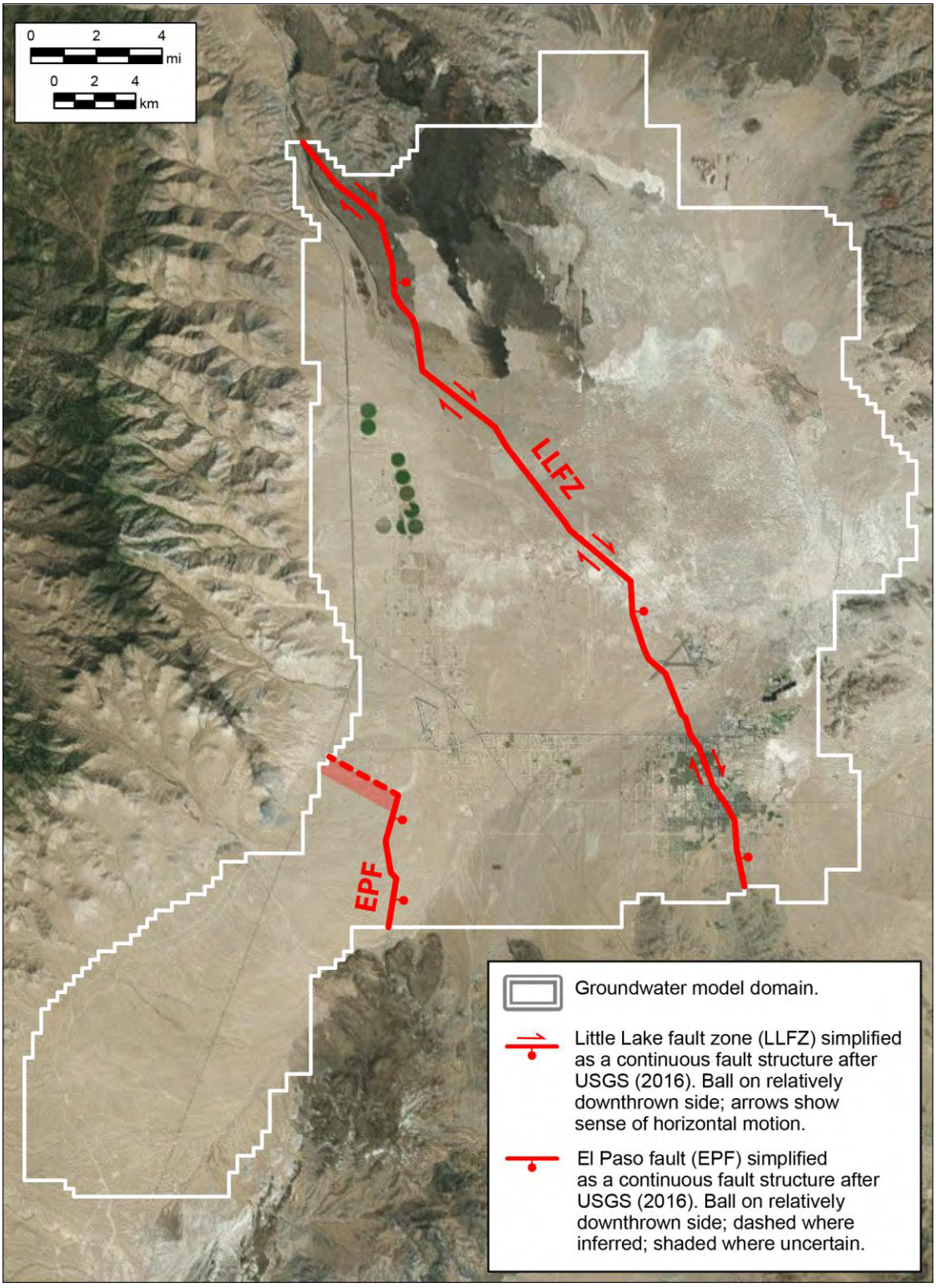

Figure 2. Map of the Indian Wells Valley groundwater model domain showing the location of the Little Lake and El Paso fault zones (LLFZ and EPF, respectively). There is some uncertainty in the location of the northwest trending portion of the EPF, which is why it is dashed and represented in red shading.

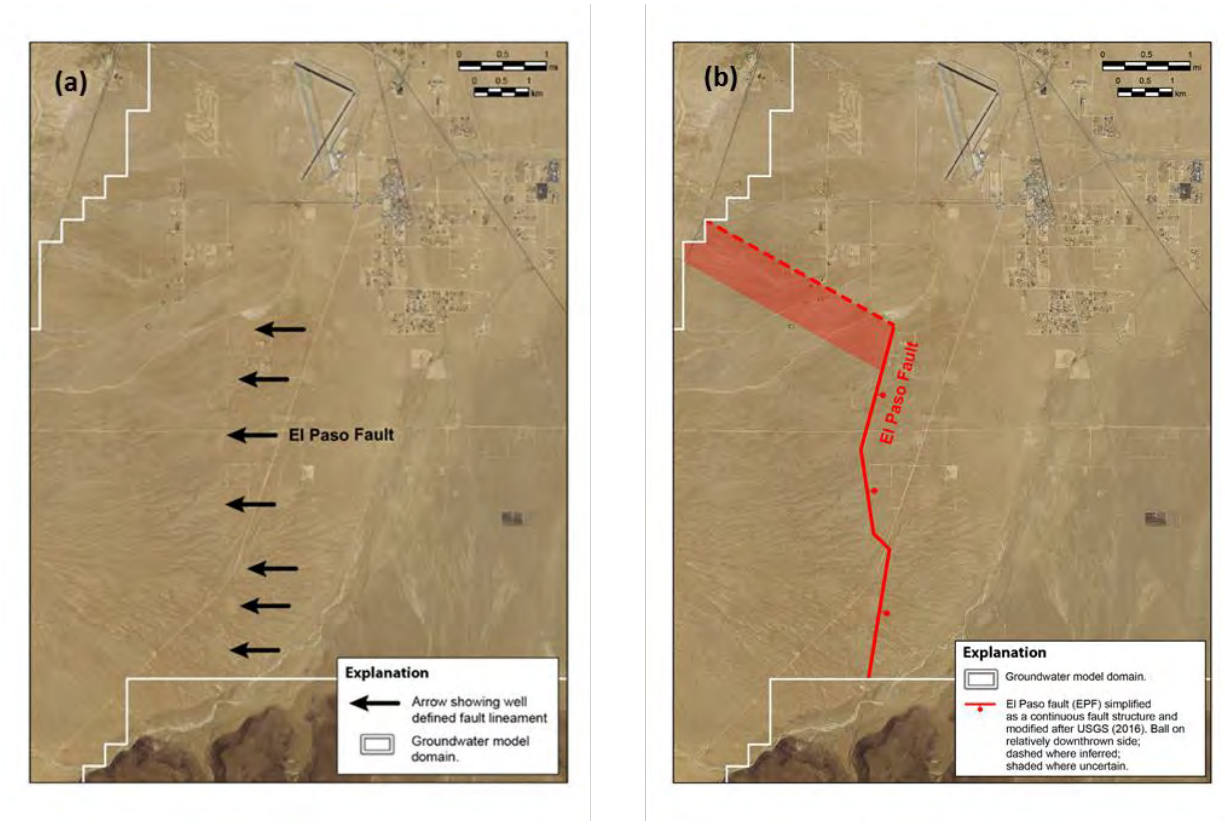

Figure 3. Maps showing the location of the informally named El Paso Fault (EPF) previously mapped as an unnamed fault by USGS (2016). Map (A) shows the location of a well-defined lineament that displaces the surface of a likely late Pleistocene alluvial fan; and (B) shows the orientation of the EPF as a continuous fault structure that steps left to connect with Sierra Nevada front faults mapped by USGS (2016) outside of the model domain (see Figure 2). The dashed section of fault is inferred to be concealed by younger alluvial fan deposits of likely Holocene age. The location and strike of the inferred section of fault is based on the position of the local groundwater level from nearby wells east of the mapped fault trace, but there is some uncertainty as to its exact location which is why it is shaded.

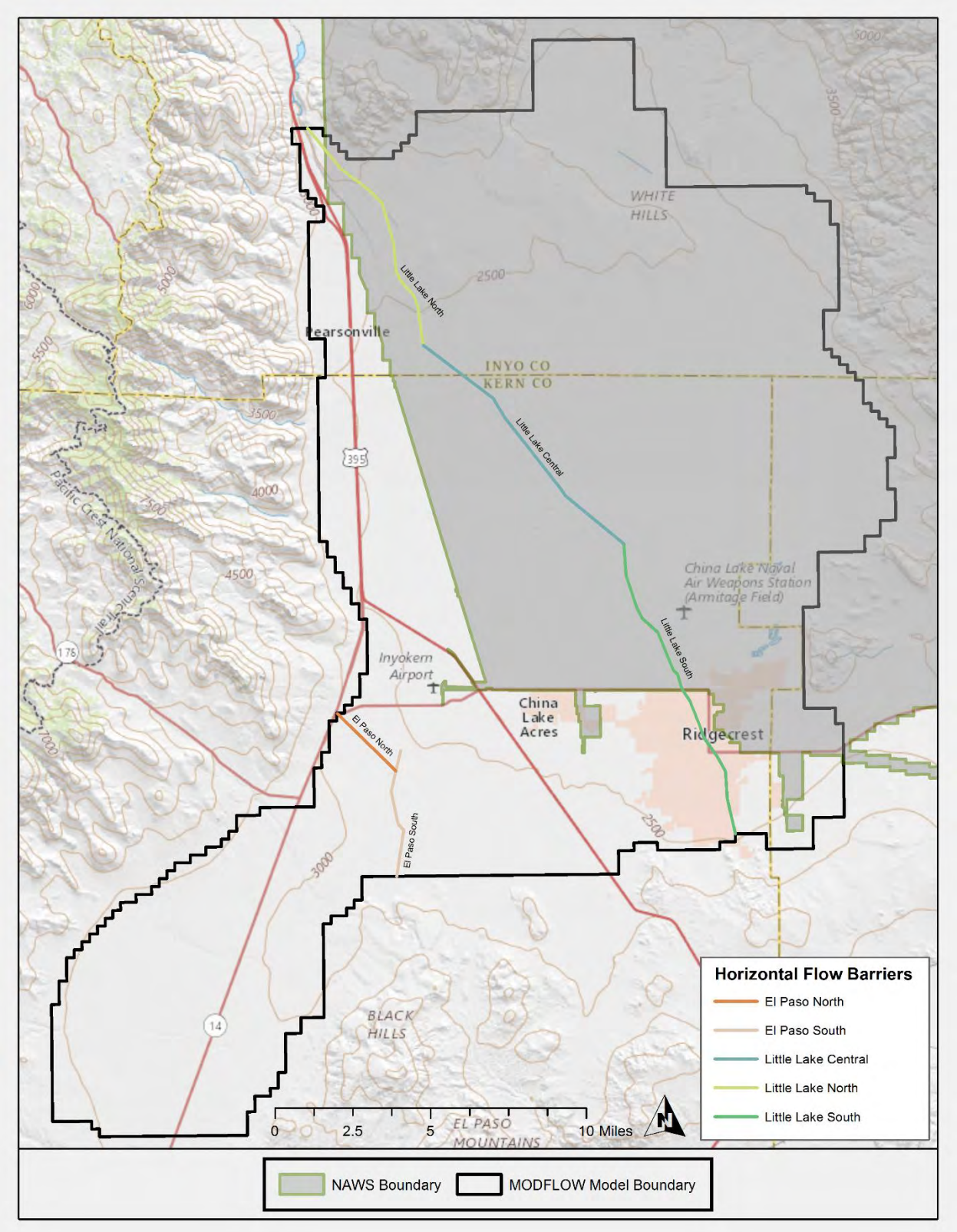

Figure 4. Horizontal flow barriers in the revised groundwater flow model. A total of five barrier segments were used with each segment having a unique hydraulic characteristic value.

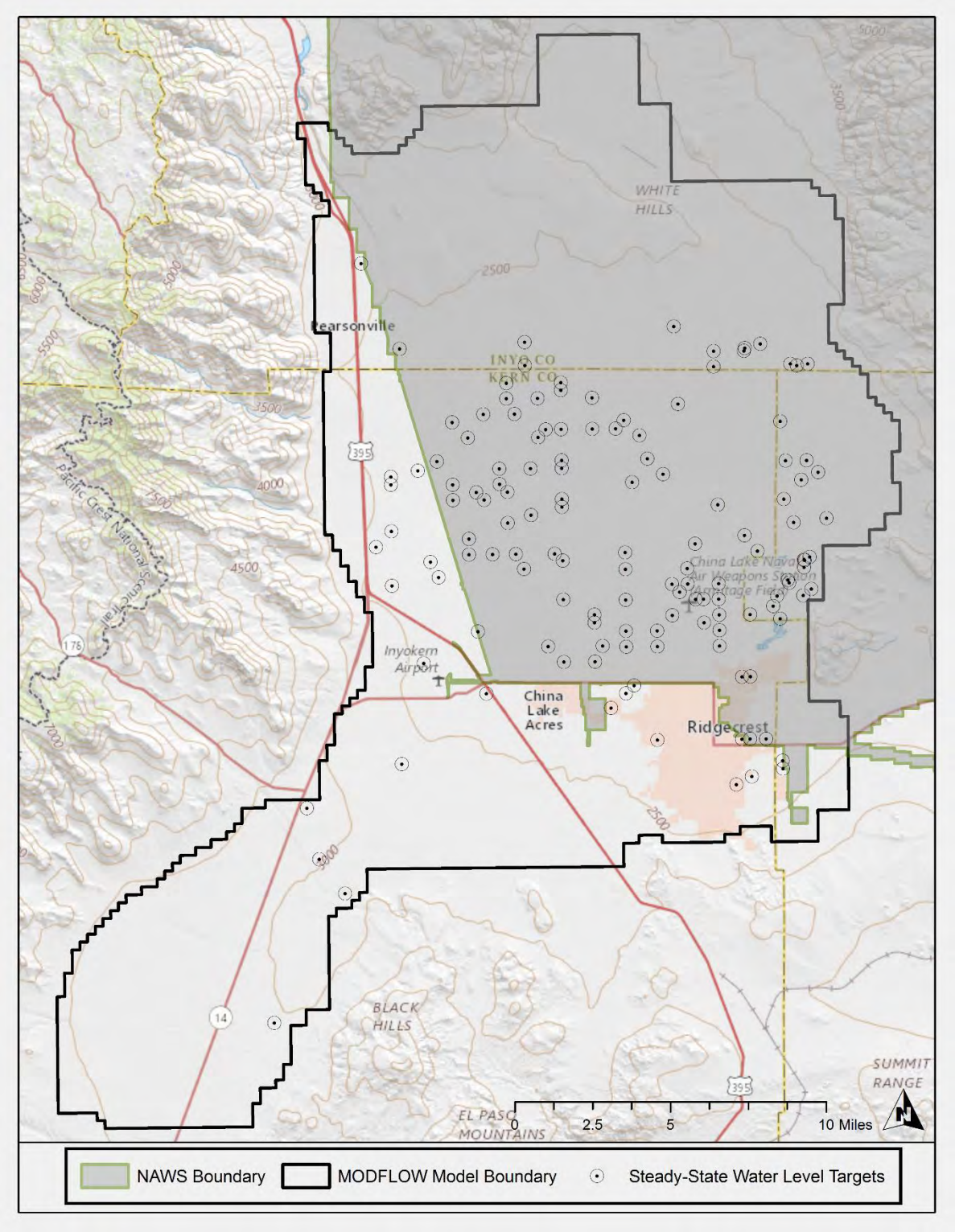

Figure 5. Location of groundwater level targets for the steady-state model.

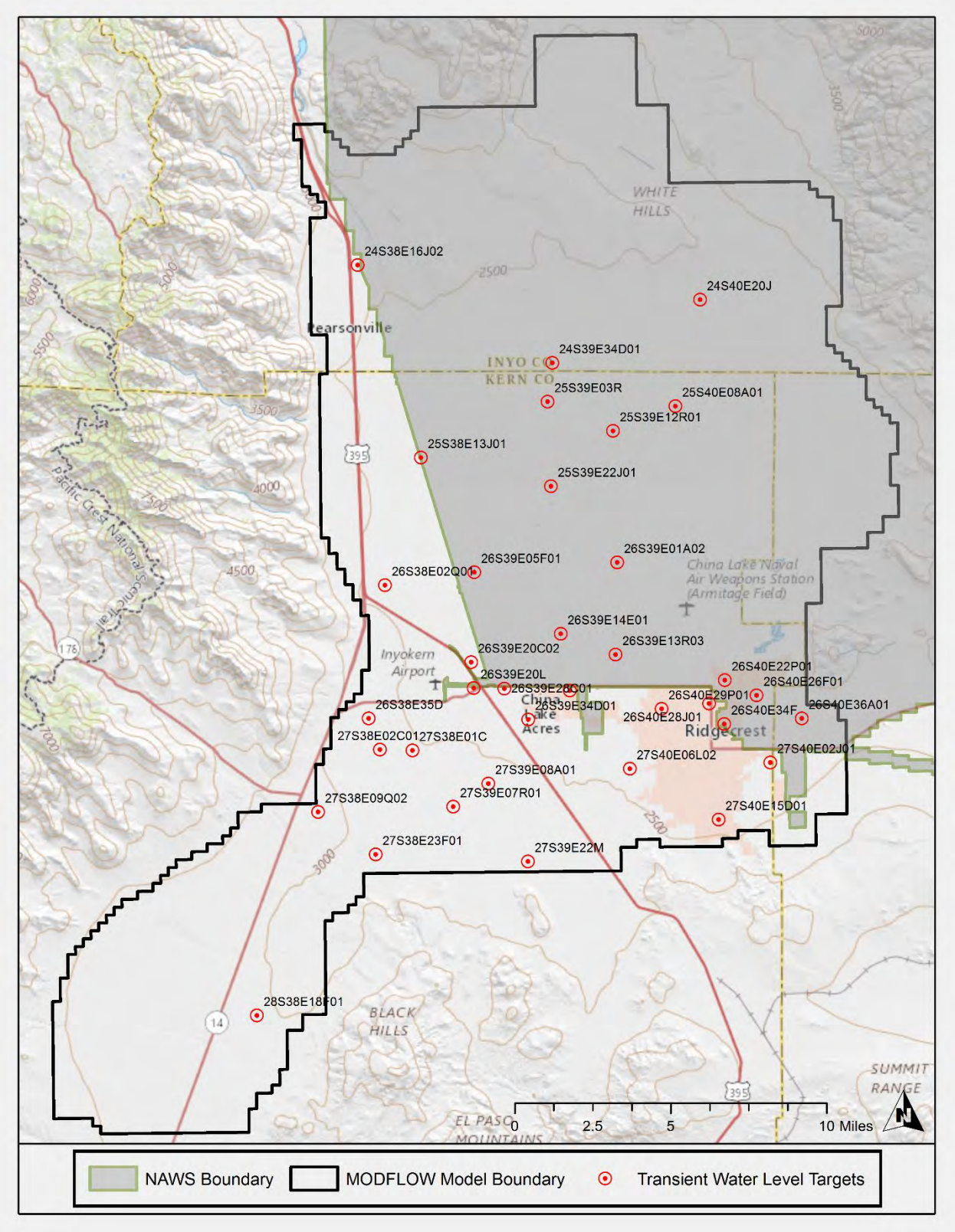

Figure 6. Location of groundwater level targets used for the transient model.

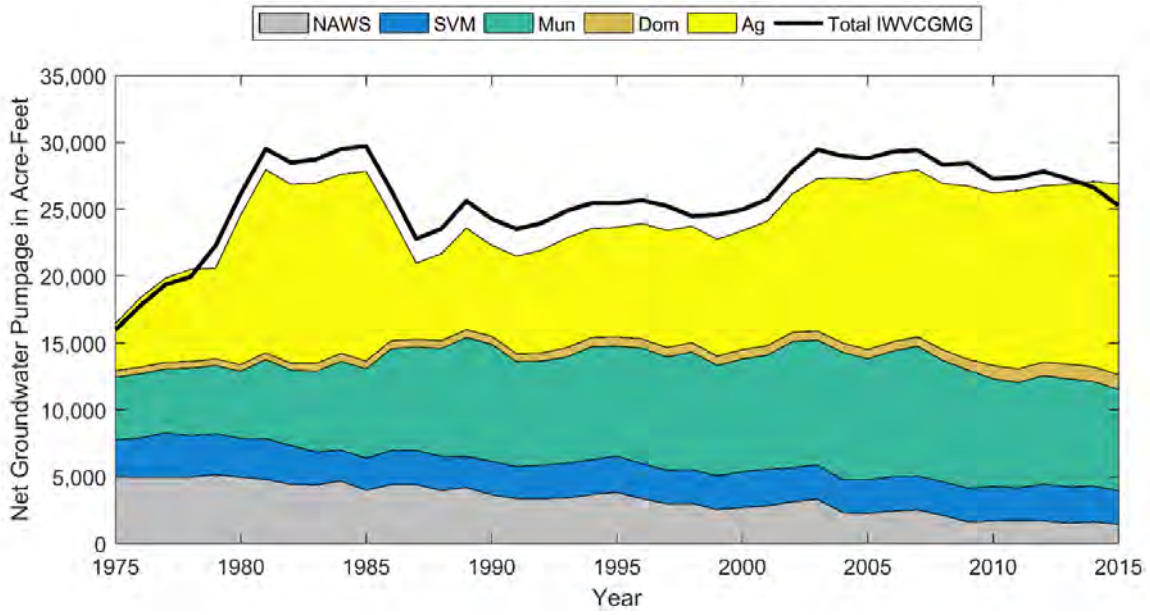

Figure 7. Groundwater production for the Naval Air Weapons Station (NAWS), Searles Valley Minerals (SVM), municipal (Mun), domestic (Dom), and agriculture (Ag) as estimated by the Indian Wells Valley Cooperative Groundwater Management Group (IWVCGMG).

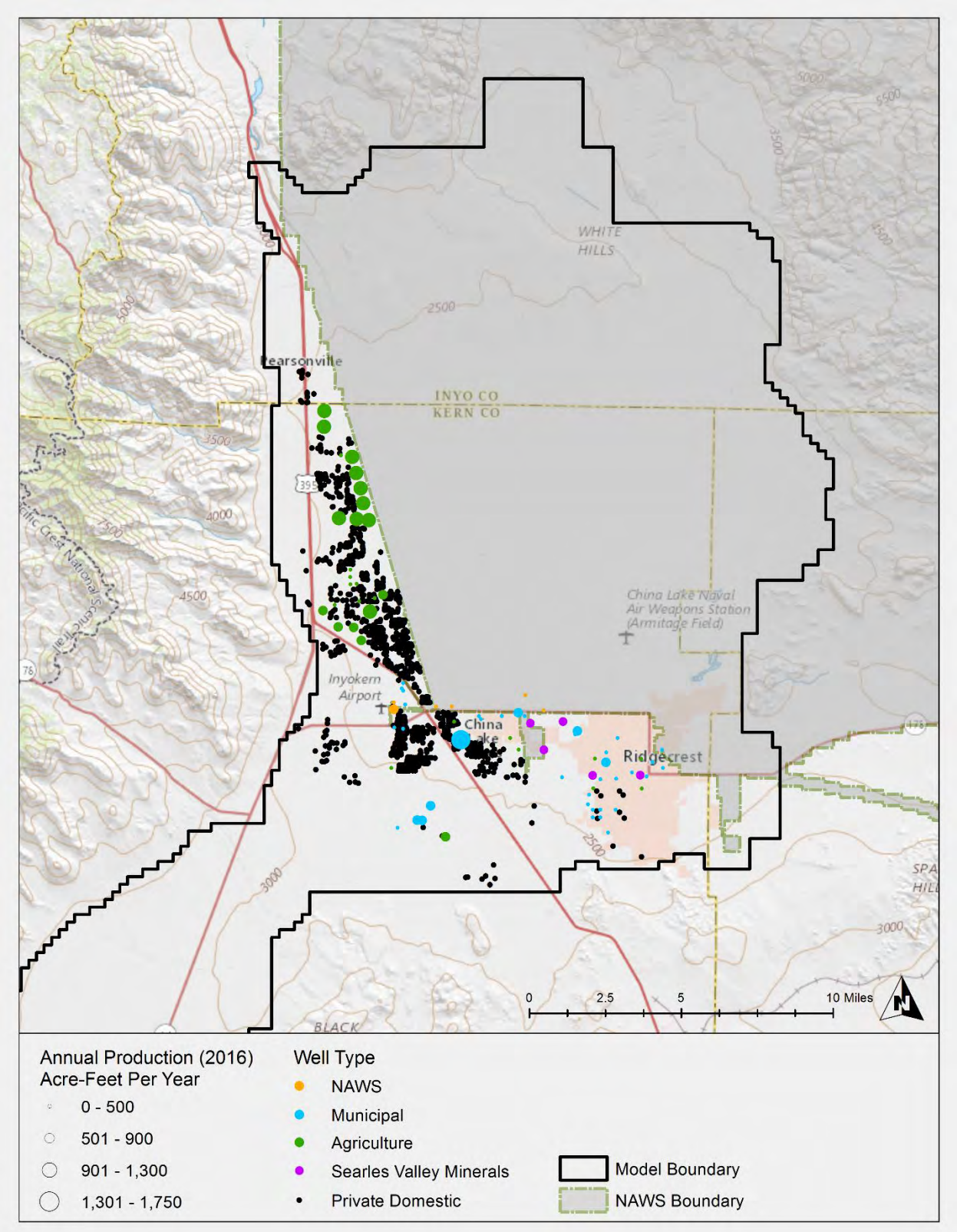

Figure 8. Groundwater extraction wells included in the transient model.

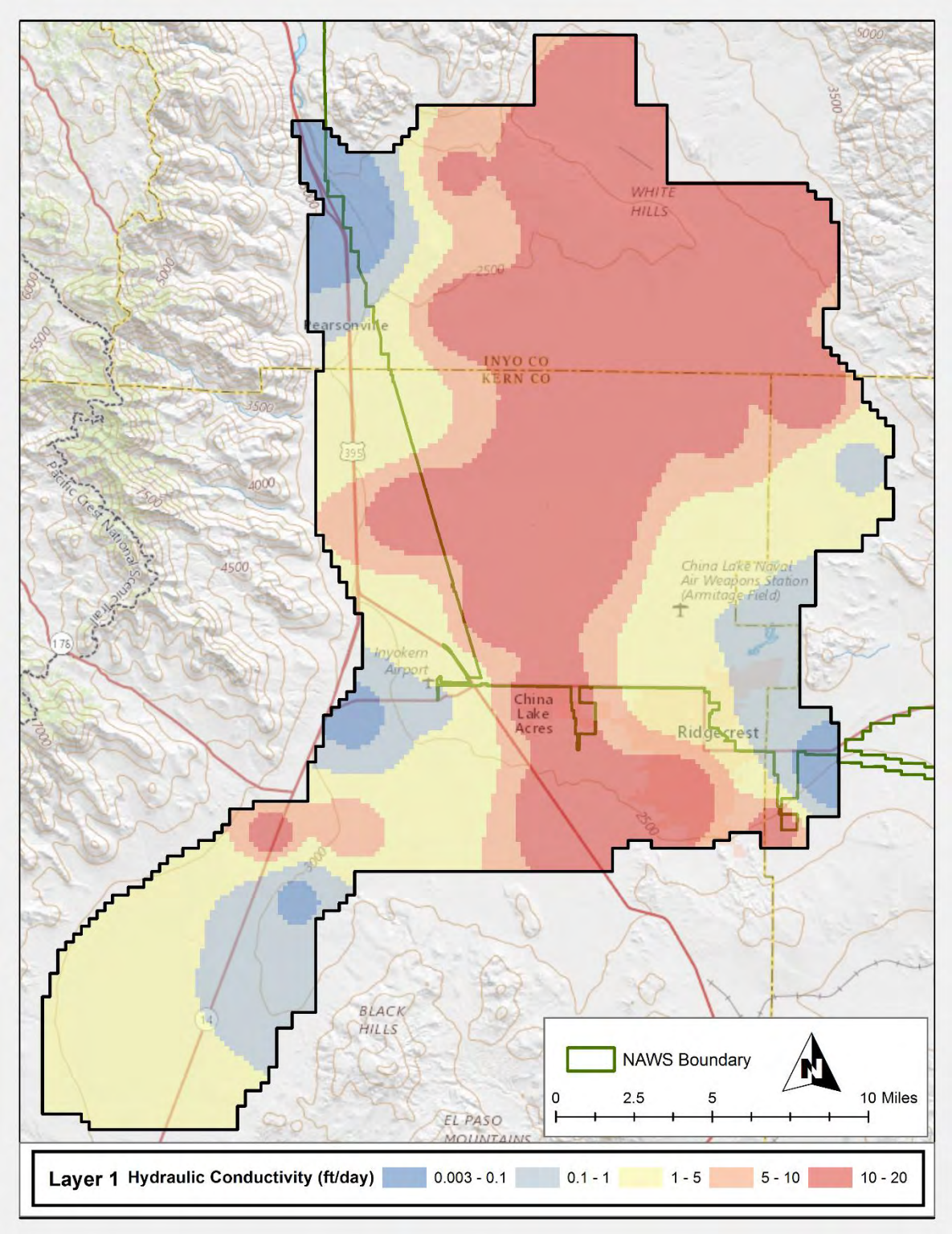

Figure 9. Calibrated hydraulic conductivity field (layers 1 – 3).

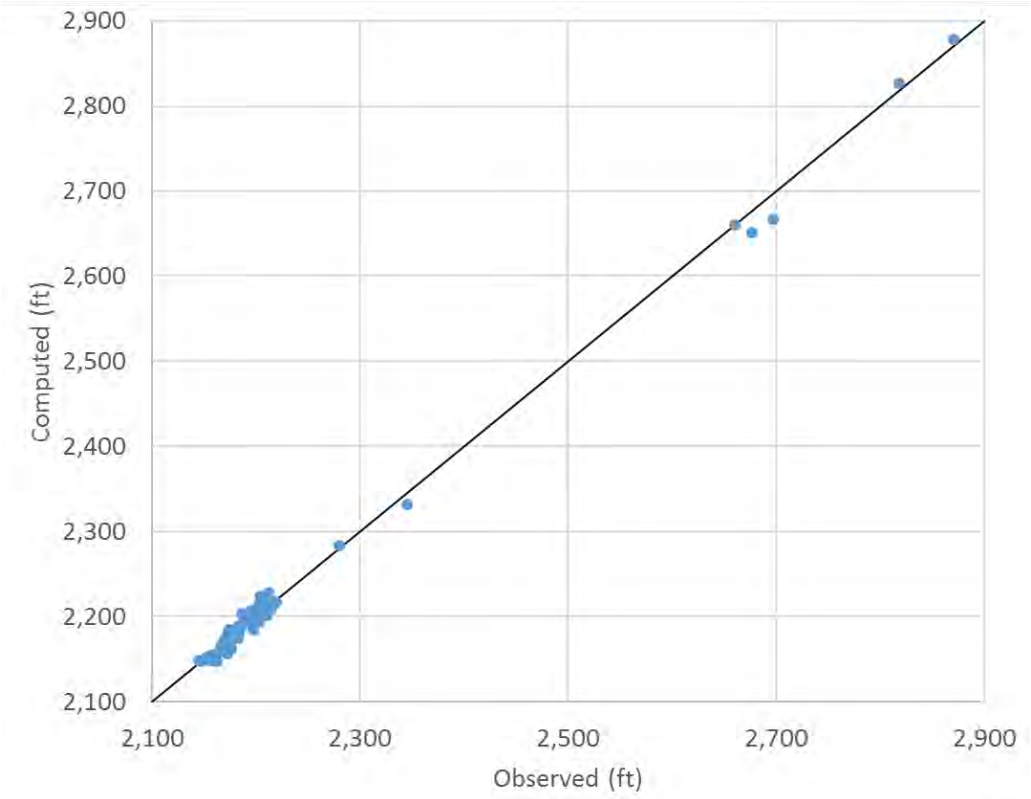

Figure 10. Observed versus computed groundwater levels for the steady-state model.

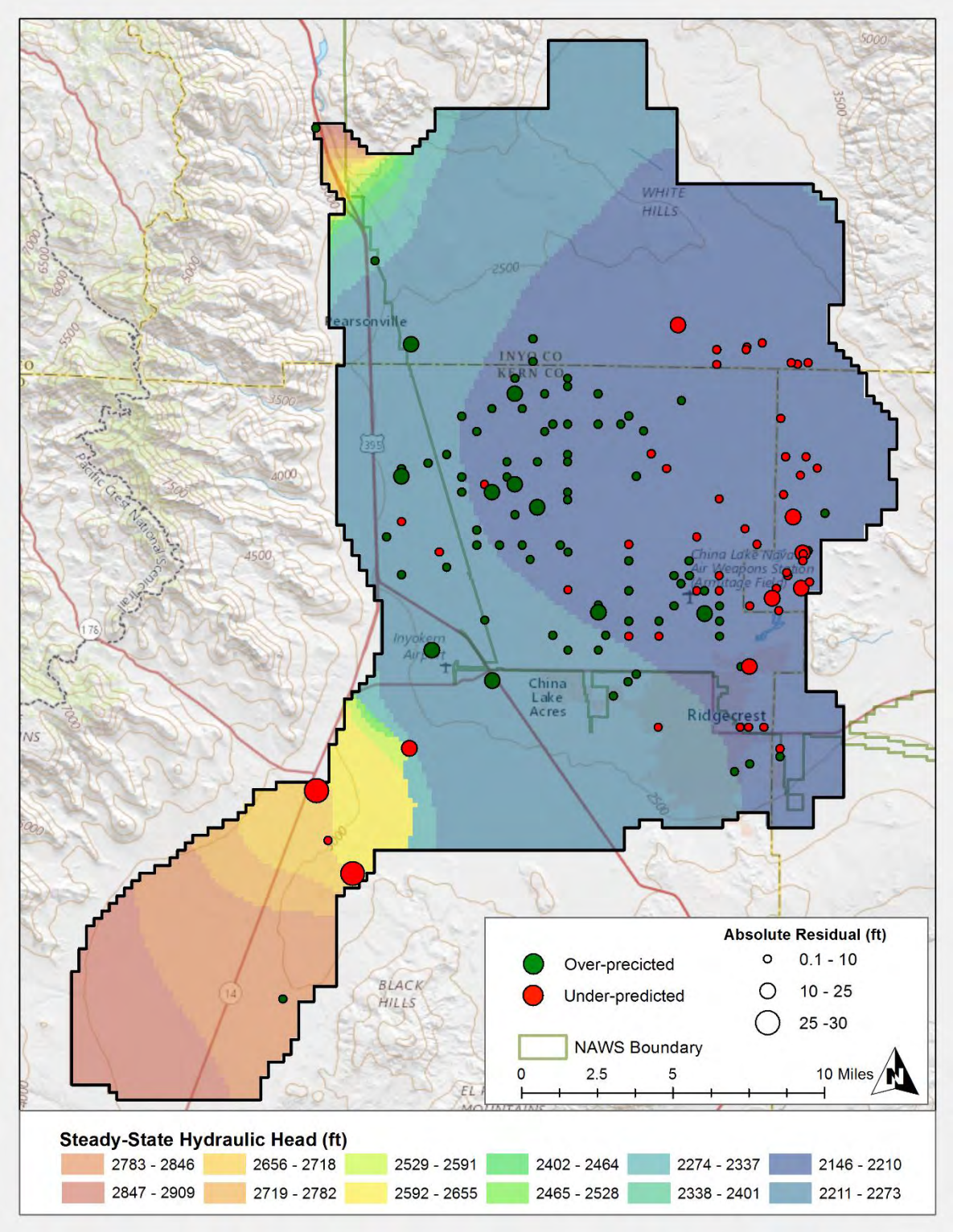

Figure 11. Residual in the simulated versus observed groundwater level for the steady-state model. Green dots indicate simulated head greater than the observed and red dots indicate simulated head less than the observed. The size of the dots is proportional to the absolute residual.

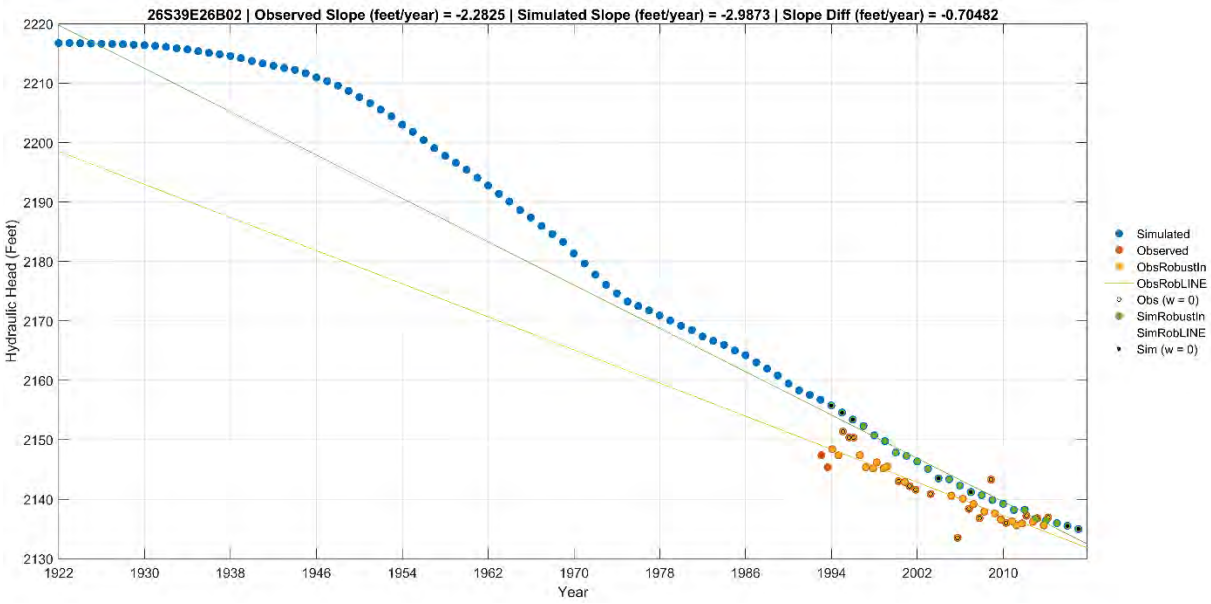

Figure 12. Example plot of time versus hydraulic head for well 26S39E26B02. Red dots represent the observed water levels, blue the simulated water levels, yellow and green represent the observed and simulated water levels that were inputs to the regression model, and hollow black dots and solid black dots correspond to outliers identified in the observed and simulated, respectively.

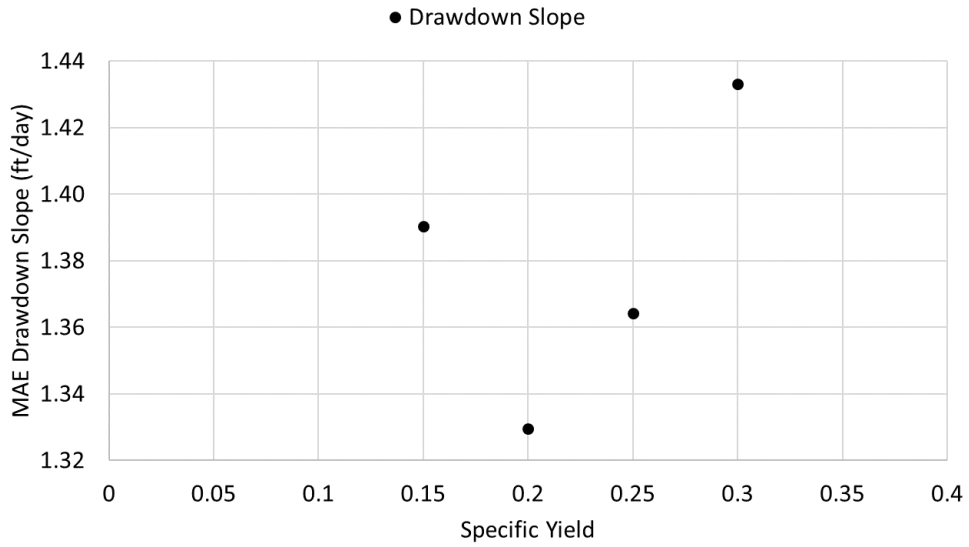

Figure 13. Mean absolute error (*MAE*) in the drawdown slope for various specific yield values.

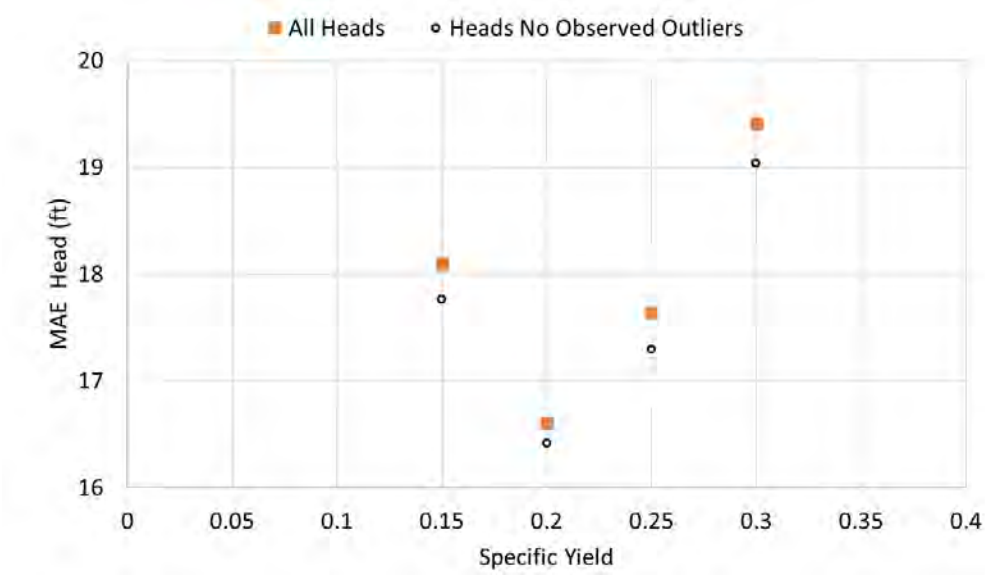

Figure 14. Mean absolute error (*MAE*) in the hydraulic head (groundwater level) for various specific yield values.

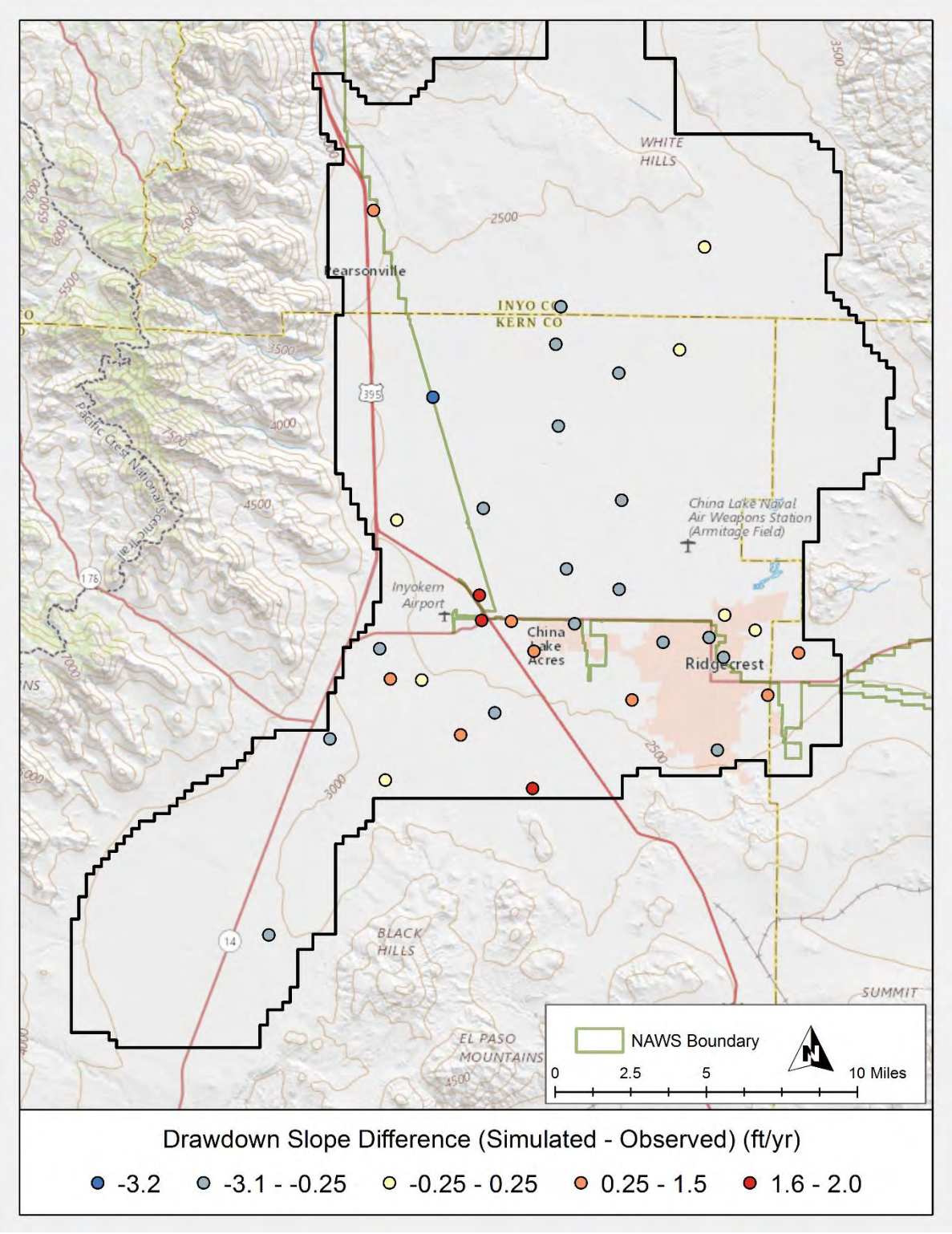

Figure 15. Difference in the drawdown slope (simulated – observed) for the transient calibration model.

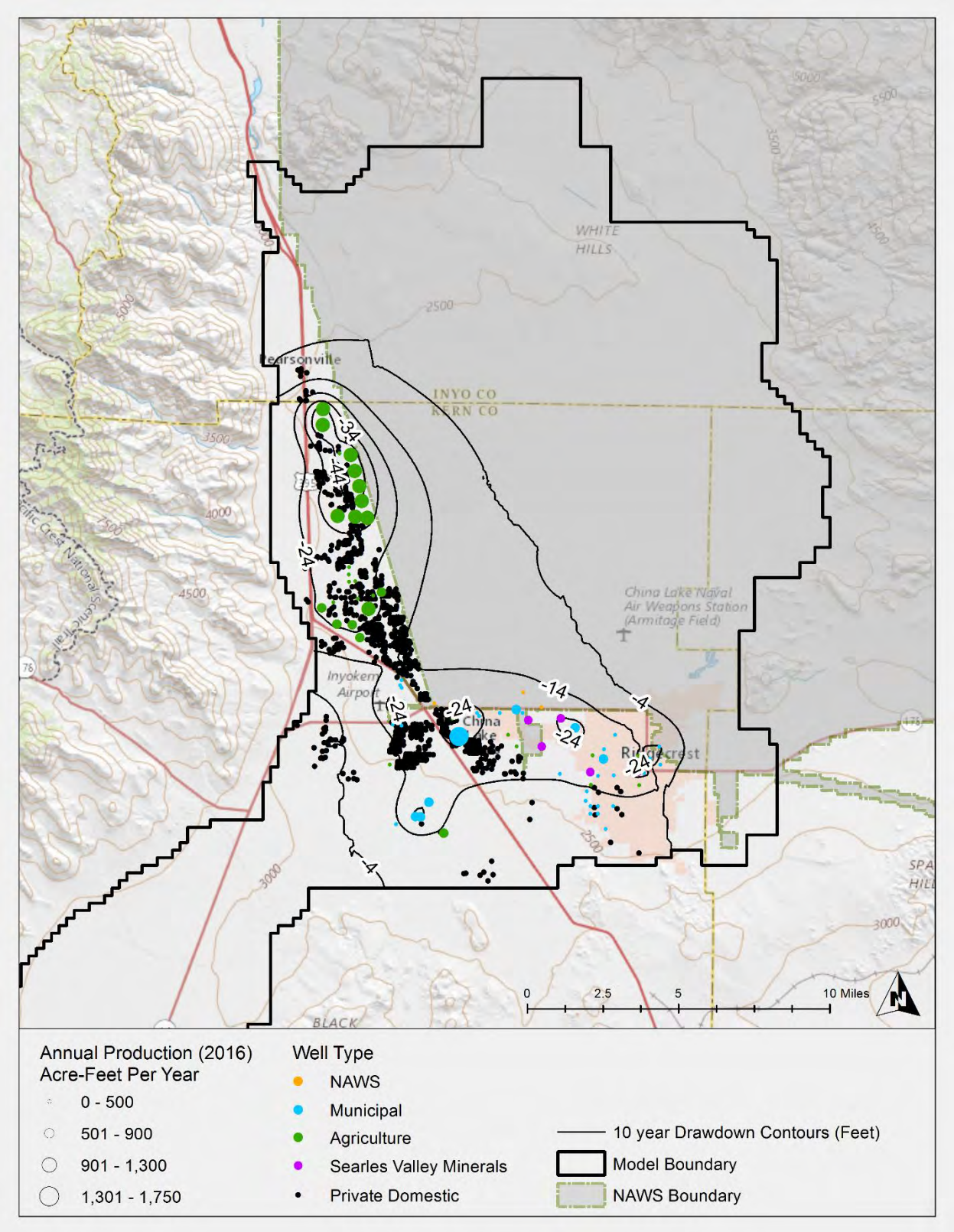

Figure 16. Simulated drawdown in 2027 (10 years).

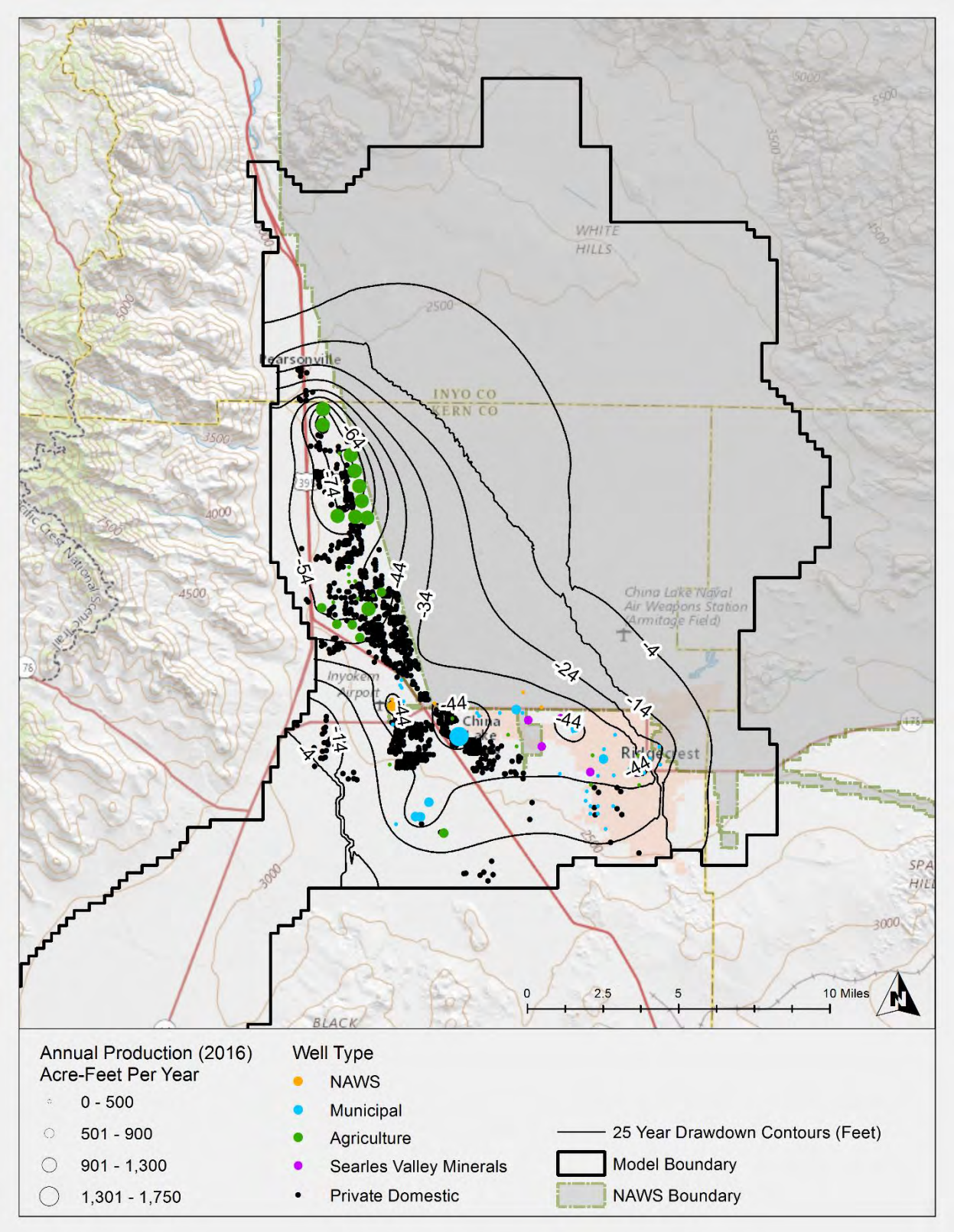

Figure 17. Simulated drawdown in 2042 (25 years).

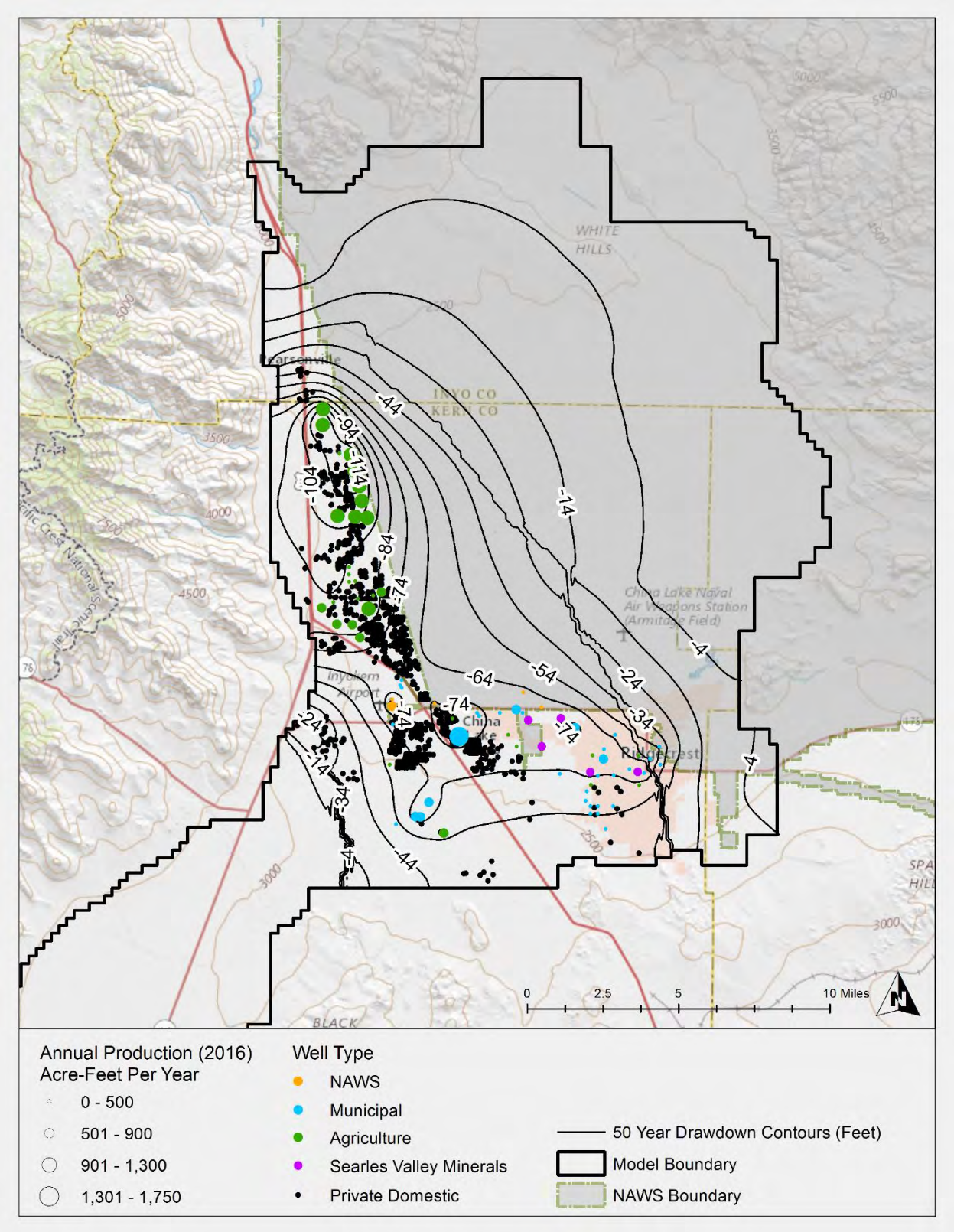

Figure 18. Simulated drawdown in 2067 (50 years).

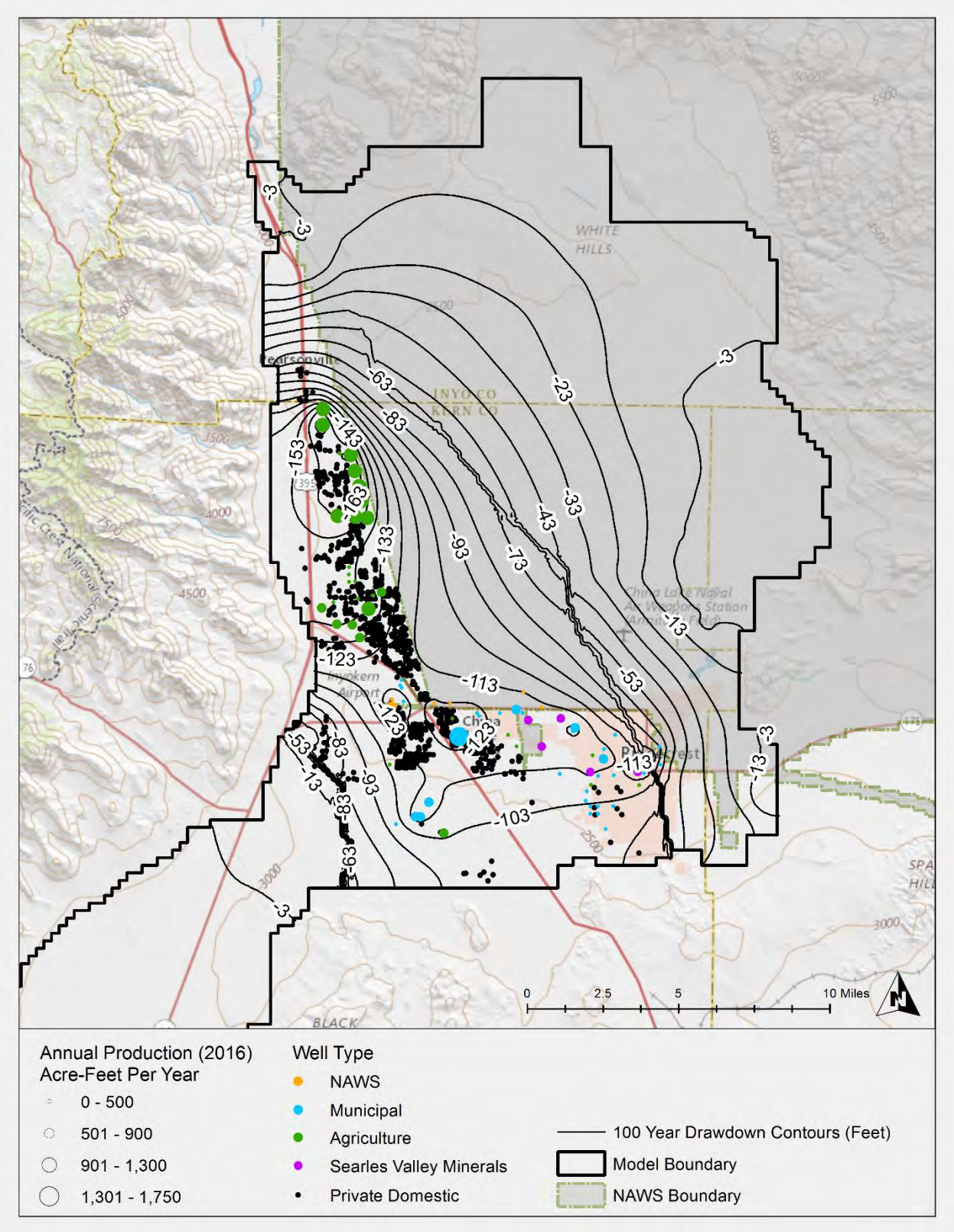

Figure 19. Simulated drawdown in 2117 (100 years).

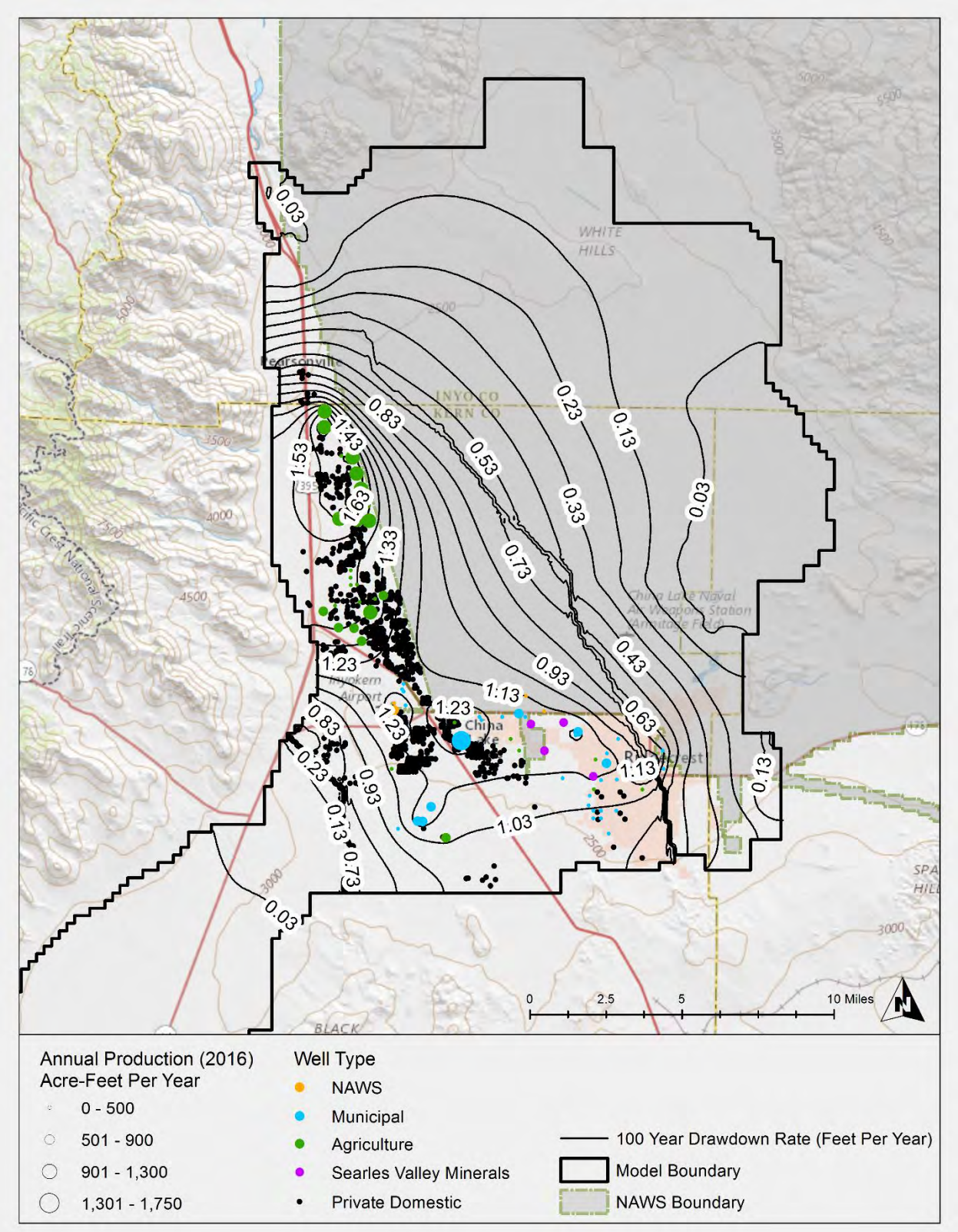

Figure 20. Simulated drawdown rate in 2117 (100 years).

Appendix A: Transient Simulated Hydrographs